

State determination of composite systems of two spatial qubits

G. Lima,¹ F. A. Torres-Ruiz,² Leonardo Neves,¹ A. Delgado,² C. Saavedra,² and S. Pádua^{1,*}

¹*Departamento de Física, Universidade Federal de Minas Gerais,
Caixa Postal 702, Belo Horizonte, MG 30123-970, Brazil.*

²*Center for Quantum Optics and Quantum Information, Departamento de Física,
Universidad de Concepción, Casilla 160-C, Concepción, Chile.*

(Dated: May 26, 2019)

Abstract

In a recent letter [Phys. Rev. Lett. 94, 100501 (2005)], we presented a scheme for generating pure entangled states of spatial qudits using transverse correlations of parametric down-converted photons. Here we show how the modification of this scheme can be used to generate spatial mixed states of qudits. We have also experimentally implemented a protocol for a full quantum tomographic reconstruction for the case of a mixed state of two spatial qubits. The protocol is based on local operations acting on the spatial qubits, which are given by natural propagation of the qubits and a suitable positioning of the photon detectors for the measurement in coincidence. This scheme can be generalized to the case of mixed state of spatial qudits.

PACS numbers: 03.67.Mn, 03.65.Wj

*Electronic address: spadua@fisica.ufmg.br

I. INTRODUCTION

The quantum state is considered to be the most complete description available of an individual physical system. The statistical distributions of the observables of a given system are completely characterized by its state. Therefore, the development of techniques to perform the state determination is of the upmost importance because they allow us to predict the results that are more likely to happen for any further possible measurement. Beside this fact, the explorations of new technological fields is bringing more motivations for the study of these techniques. In Quantum Information, for example, protocols like teleportation [1] and superdense coding [2] require initially knowing the quantum state to be implemented. Another special case is the use of reconstructed density matrices to calculate quantities such as the concurrence [3] of a composite system.

Several techniques have been used for the state estimation of different physical systems. In the field of atomic physics, quantum endoscopy was used to determine the state of ions and atoms [4, 5, 6]. In quantum optics, the Wigner function of multi mode fields could be measured using the homodyne detection [7, 8, 9] and the technique of quantum tomographic reconstruction (QTR) was used for measuring the polarization state of the parametric down-converted photons [10].

In general, these methods are based on a linear inversion of the measured data. In the case of QTR, the data is acquired with a series of measurements performed on a large number of identically prepared copies of a quantum system. The fact that this transformation is linear, makes it strongly dependent of any experimental errors that may occur while recording the data. They can appear as a consequence of the experimental noise or misalignment and therefore, the reconstructed state is only a reasonable approximation of the real quantum state. The density matrices obtained may have properties that are not fully compatible with a quantum state. Another alternative that has been considered for the state determination is the numerical technique called maximum likelihood estimation [11, 12]. It is based on a relation between the measured data and the quantum state that could have generated them. Even though it generates only the possible density matrices, it has the drawback of enhancing the uncertainty on the state estimation.

Spontaneous parametric down-conversion (SPDC) is a nonlinear optics process where one photon from the pump(p) laser beam incident to a crystal can originate two other photons,

signal(s) and idler (i)[13]. The generated photon pairs are also called twin photons for being generated simultaneously with a very small temporal uncertainty [14]. We have recently demonstrated that it is possible to use the transverse correlations of the photon pairs, produced during the SPDC process, to generate pure entangled states of higher \mathcal{D} -dimensional Hilbert space, with $\mathcal{D} > 2$, known as qudits [15, 16, 17]. Because the quantum space of these photons is defined by the number of different available ways for their transmission through apertures placed in their path, we call them spatial qudits. In the present work, we first discuss how a modification of the setup employed to create pure qudit entangled states can be used to generate mixed states. The study of mixed states is an important field of research because it allows one to consider more realistic experimental situations where a pure state due to interactions with its environment becomes a mixture of quantum systems. Following this, we investigate the state determination of a system composed of two mixed states of spatial qubits ($\mathcal{D} = 2$). We emphasize on this type of system because they are good candidates for being used in quantum communication. Therefore, a procedure for their characterization is of upmost importance. We show here that it is possible to perform the QTR for a mixed state of two spatial qubits by experimentally reconstructing the density matrix of a system composed of two spatial qubits. The quality of the reconstruction is also discussed. Even though we considered just this special case it is straightforward to show that the technique used can be generalized for being applied to a system composed of two spatial qudits in mixed state.

II. CONTROLLED GENERATION OF MIXED STATES

References [15, 16] show that the state of parametric down-converted photons when transmitted through identical multi slits, with d being the distance between two consecutive slits and a , the half width of the slits, can be written as

$$|\Psi\rangle \propto \sum_{l=-l_D}^{l_D} \sum_{m=-l_D}^{l_D} W_{lm} e^{i \frac{kd^2}{8z_A} (m-l)^2} |l\rangle_s \otimes |m\rangle_i, \quad (1)$$

where $l_D = (D - 1)/2$, and D is the number of slits in these apertures. The function W_{lm} is the spatial distribution of the pump beam at the plane of the multi slits ($z = z_A$) and at the transverse position $x = (l + m)d/2$,

$$W_{lm} = W \left[\frac{(l+m)d}{2}; z_A \right]. \quad (2)$$

The $|l\rangle$ (or $|m\rangle$) state, is a single-photon state defined, up to a global phase factor, by

$$|l\rangle_j \equiv \sqrt{\frac{a}{\pi}} \int dq_j e^{-iq_j ld} \text{sinc}(q_j a) |1q_j\rangle, \quad (3)$$

and represents the photon in mode j ($j = i, s$) transmitted by the slit l . q_j is the transverse component of wave vector of the down-converted photons. The base $\{|l\rangle_j\}$ satisfies $\langle l | l' \rangle_j = \delta_{ll'}$. We use these states to define the logical states of the qudits and thus, it is clear that Eq. (1) represents a composite system of two qudits. The qudits are represented by a vector in the Hilbert space which the dimension is D because the degree of freedom of each photon are the available paths for their transmission through the multi slits.

It can be seen from Eq. (1) and Eq. (2), that it is possible to create different pure states of spatial qudits if one knows how to manipulate the pump beam in order to generate distinct transverse profiles at the plane of the multi slits ($W(\xi; z_A)$). In Ref. [16], we showed experimentally that a maximally entangled state of spatial ququarts ($D = 4$)

$$|\Psi\rangle = \frac{1}{2} \sum_{l=-\frac{3}{2}}^{\frac{3}{2}} e^{ik\frac{d^2 l^2}{2z_A}} |l\rangle_s \otimes |-l\rangle_i, \quad (4)$$

can be generated when the pump beam is focused at the plane of two identical four-slits in such a way that it is non vanishing except at a region smaller than the dark part of these apertures. The state in Eq. (4) shows the correlation between the photons such that, when the photon in mode s is transmitted by the slit l , the photon in mode i will pass through the symmetrically opposite slit $-l$. In this experiment, a non-linear crystal was directly pumped by a krypton laser beam. A lens having a small focal length was used before this crystal to focus the pump beam.

Let us assume that, before reaching the crystal, the pump beam pass through an unbalanced Mach-Zehnder interferometer where the transverse profile of the laser beam is modified differently in each arm. If the difference between the lengths of these arms is set larger than the laser coherence length, we will obtain an incoherent superposition of the states generated by each arm. It is interesting to note that this generation of mixed states of spatial qudits can be completely controlled. Besides the fact that we can control the states generated by

each arm, we also can control the probabilities for generating them by placing attenuators at the interferometer arms.

In the following section, we show how to use the QTR technique to determine the density matrix of this composite system. The state whose the density matrix is reconstructed is a mixed state of the spatial qubits. This state is generated with the experimental setup represented in Fig. 1(a). A 5 mm β -barium borate crystal is pumped by a 500 mW krypton laser emitting at $\lambda = 413$ nm for generating SPDC. Before being incident at the crystal, the pump beam cross an unbalanced Mach-Zehnder interferometer. The difference between the lengths of each interferometer arm (200 mm) is set larger than the laser coherence length (80 mm). Two identical double slits A_s and A_i are aligned in the direction of the signal and idler beams, respectively, at a distance of 200 mm from the crystal (z_A). The slits' width is $2a = 0.09$ mm and their separation, $d = 0.18$ mm. At the arm 1 of the interferometer, we place a lens that focus the laser beam at the plane of these double slits, into a region smaller than d . In arm 2, we use a set of lenses that increases the transverse width of the laser beam at z_A . The transverse profiles generated are illustrated in Fig. 1(a). The photons transmitted through the double-slits are detected in coincidence between the detectors D_i and D_s . Two identical single slits of dimension 5.0 x 0.1 mm and two interference filters with 8 nm full width at half maximum (FWHM) bandwidth are placed in front of the detectors.

Using Eq. (1) and Eq. (2), we can show that the two-photon state, after the double slits, when only arm 1 is open is given by

$$|\Psi\rangle_1 = \frac{1}{\sqrt{2}}(|+\rangle_s|-\rangle_i + |-\rangle_s|+\rangle_i). \quad (5)$$

To simplify, we used the state $|+\rangle_j$ ($|-\rangle_j$) to represent the j photon being transmitted by the upper (lower) slit of the respective double slit. The state shown in Eq. (5) is a maximally entangled state of two spatial qubits. However, if the laser beam cross only arm 2, the state of the twin photons transmitted by the apertures will be a state of the type is given by

$$\begin{aligned} |\Psi\rangle_2 = & \frac{1}{2}e^{i\phi}(|-\rangle_s|+\rangle_i + |+\rangle_s|-\rangle_i) \\ & + \frac{1}{2}(|-\rangle_s|-\rangle_i + |+\rangle_s|+\rangle_i), \end{aligned} \quad (6)$$

where $\phi = \frac{kd^2}{8z_A}$. Therefore, the two-photon state generated in our experiment when the two arms are liberated, is a mixed state of the spatial maximally entangled state of Eq. (5) and

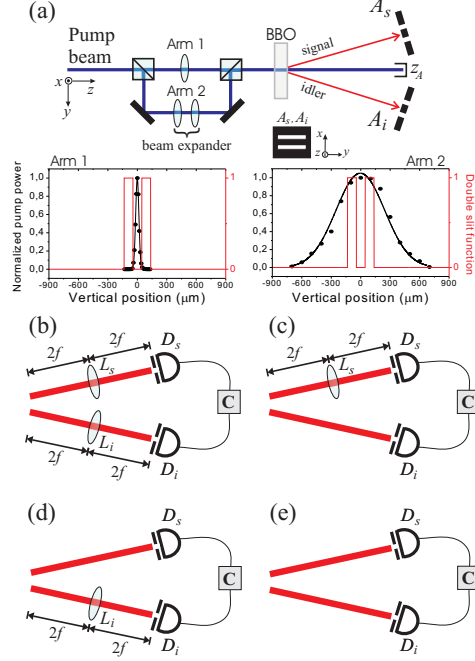


FIG. 1: (a) Schematic diagram of the experimental setup used for generating and characterizing the mixed states of spatial qubits. The pump beam that cross arm 1 is focused in a narrow region at Z_A or in a broader spatial region when it cross arm 2 (Graphs: Arm1 and Arm 2). A_s and A_i are the double-slits at signal and idler propagation paths, respectively. D_s and D_i are detectors and C is a photon coincidence counter. The configuration used to determine the diagonal elements is represent in (b). (c) and (d) were used for the second type of measurement and (e) for the third type.

the state of Eq. (6). It is described by the density operator

$$\rho_{\text{the}} = A|\Psi\rangle_{11}\langle\Psi| + B|\Psi\rangle_{22}\langle\Psi|. \quad (7)$$

where A and B are the probabilities for generating the states when the pump beam pass by arm 1 and arm 2, respectively.

III. RECONSTRUCTION

Now, we show how QTR can be experimentally implemented to reconstruct the density matrix of the state generated in our experiment, given by Eq. (7), without the use of any information about this generation.

The process of quantum tomography, which is described in Refs. [18, 19], is easy to be understood. The first thing to remark is the fact that it is always possible to measure the diagonal elements of any density operator, directly. Therefore, the quantum tomographic reconstruction is just a protocol to determine the non diagonal ones. It consists in the use of local operations at the subsystems to allow their detection in different basis. Since the form of the global density operator depends on the basis of the subsystem detected at, the effect of these local operations is the generation of new global density operators. Because we know which were the change of basis performed by the local operations, we can relate the diagonal elements (that are measurable) of a new density matrix, say $\tilde{\rho}$, with the non diagonal ones (that are not measurable) of the original density operator, ρ . If we repeat this procedure to obtain more density operators and measure their diagonal, we will create a set of independent equations which allows the determination of the non diagonal elements of ρ .

To characterize the state generated in our experiment, we first adopt a general form for its density matrix

$$\rho = \begin{bmatrix} \rho_{++++} & \rho_{+---} & \rho_{-+++} & \rho_{--++} \\ \rho_{+++-} & \rho_{+-+-} & \rho_{-++-} & \rho_{--+-} \\ \rho_{++-+} & \rho_{+---} & \rho_{-++-} & \rho_{--++} \\ \rho_{+-+-} & \rho_{+---} & \rho_{-++-} & \rho_{----} \end{bmatrix}, \quad (8)$$

where $\rho_{j_s j_i k_s k_i} = \langle j_s j_i | \rho | k_s k_i \rangle$ and $j, k = \pm$.

A. Diagonal Elements

The diagonal elements can be determined by coincidence measurements with the detectors just behind the double slits [16] or, equivalently, at the plane of the image formation of these apertures when two lenses are placed in the signal and idler paths, as showed in Fig. 1(b) [20]. In these measurements, one detector is kept fixed behind one slit while the other detector scans the x direction over the entire region of the second double slit. Two measurements of this type, are shown in Fig. 2, with detector D_i going from slit “+” to the slit “-”. When the detector D_s is at position $x = 100 \mu\text{m}$ ($x = 300 \mu\text{m}$), it detects all photons that cross the slit “-” (“+”). By using these four coincidence numbers measured when D_s is at the position $x = 100 \mu\text{m}$ or $x = 300 \mu\text{m}$ and D_i is fixed behind the slit “+” (Fig. 2(a)) or

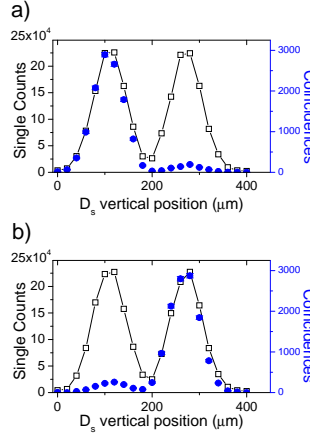


FIG. 2: D_s single counts (□) and coincidence counts (●) measured in 20 s, simultaneously, with D_i fixed behind one of the slits of its aperture. In (a), D_i is fixed behind the slit “+” and in (b) it is fixed behind slit “-”. The slits’ width of the double-slit is $2a = 0.09$ mm. The slits’ width of the single slits placed at the detector is $2a = 0.10$ mm. When the detector D_s is at position $x = 100$ μm ($x = 300$ μm), it detects all photons that cross the slit “-” (“+”).

behind the slit “-” (Fig. 2(b)), we obtain the diagonal elements of Eq. (8): $\rho_{++++} = 0.028$, $\rho_{+-+-} = 0.468$, $\rho_{-+-+} = 0.462$ and $\rho_{----} = 0.042$. Therefore, only four points of Fig. 2 were used for obtaining the diagonal elements of Eq. (8).

B. Change of Basis

As mentioned above, for the reconstruction process it is necessary that local operations are applied in the subsystems to change the base used for writing the global density operator. What is interesting in the use of the spatial qubits is that these local operations occur naturally while they freely evolve in the space after the double slits. Just by varying the detector transverse position one can detect these spatial qubits in different basis. To understand this, lets first consider the expression for the two-photon state in a transverse plane at a distance $z - z_A$ from the double-slit’s plane [21]

$$\begin{aligned}
 |\Psi\rangle_z \propto & W(d; z_A) |g_+\rangle_s |g_+\rangle_i \\
 & + W(-d; z_A) |g_-\rangle_s |g_-\rangle_i \\
 & + W(0; z_A) (|g_+\rangle_s |g_-\rangle_i + |g_-\rangle_s |g_+\rangle_i),
 \end{aligned} \tag{9}$$

where the normalized state $|g+\rangle_j$ (or $|g-\rangle_j$) is given by

$$|g_{\pm}\rangle_j \equiv \sqrt{\frac{a}{\pi}} \int dq_j e^{i[\frac{-q_j^2(z-z_A)}{2k_j}]} \times e^{\mp iq_j d} \text{sinc}(q_j a) |1q_j\rangle, \quad (10)$$

and $|g_{\pm}\rangle_j$ ($j = s, i$) represents the state of the photon in mode j , at the plane- z when it was transmitted by the slit “+” (or “-”) of the double slit. Since the photon at this plane was certainly transmitted by one of these two slits and since the states $|g_{\pm}\rangle$ form an orthonormal base, we can use them to define the Hilbert space of this photon. For example, if we focus the laser beam at z_A , such that $W(-d; z_A) = W(d; z_A) = 0$, the state of Eq. (10) will be

$$|\Psi\rangle_z = \frac{1}{\sqrt{2}} (|g_+\rangle_s |g_-\rangle_i + |g_-\rangle_s |g_+\rangle_i), \quad (11)$$

which is a maximally entangled state. In our experiment, each photon of the pair will be described as a statistical mixture of the states $|g_{\pm}\rangle$ at the plane- z .

However, suppose that detectors with small transverse apertures are placed at this plane. These apertures will then select a photon in a certain state to be detected. They play the same role, for the spatial qubit states experiment, as the polarizers play for the entangled states of polarized photons in Bell’s inequality tests [22, 23]. The state of the selected photon, which will be detected later, can then be described as

$$|h\rangle_j = f_+(x, z) |g_+\rangle_j + f_-(x, z) |g_-\rangle_j, \quad (12)$$

where

$$|_j\langle g_{\pm} | h \rangle_j|^2 = |f_{\pm}(x, z)|^2, \quad (13)$$

are the probabilities that the selected photon in the point (x, z) , have crossed the apertures “+” or “-”, respectively.

The amplitude probability $f_+(x, z)$ is calculated by using the electric field operator, in the paraxial approximation [24]

$$\mathbb{E} = \int dq \hat{a}(q) e^{i(qx - q^2 \frac{(z-z_A)}{2k})}, \quad (14)$$

and by calculating $\langle vac | \mathbb{E}(x, z) | \pm \rangle$. After normalizing the state of Eq. (20), we have

$$f_{\pm}(x, z) = \frac{\exp\left(i \frac{k(x \mp d)^2}{2(z-z_A)}\right) \operatorname{sinc}\left(\frac{ka(x \mp d)}{(z-z_A)}\right)}{\sqrt{\operatorname{sinc}^2\left(\frac{ka(x \mp d)}{(z-z_A)}\right) + \operatorname{sinc}^2\left(\frac{ka(x \pm d)}{(z-z_A)}\right)}}. \quad (15)$$

Therefore, by changing the transverse detector position x , we can do measurements in the subsystems in different orthonormal bases, measure experimentally the diagonal of the different ρ' operators and then reconstruct the density operator in the detection z-plane. By reconstructing ρ' , we are also reconstructing ρ , the density operator at the double-slits plane z_A , because the matrix elements of ρ' and ρ are exactly the same. We show it below. Suppose a local unitary operator U_j represents the evolution operator from state $|l\rangle_j$ to $|g_l\rangle_j$ for photon j , with $j = s, i$,

$$U_j = e^{-ik(z-z_A)} \int dq e^{i[-q^2(z-z_A)/2k]} |1q\rangle_{jj} \langle 1q|, \quad (16)$$

such that

$$|g_l\rangle_j = U_j |l\rangle_j, \quad (17)$$

with $l = +, -$. If

$$\rho = \sum_{l,m,l',m'} \rho_{l,m,l',m'} |l,m\rangle \langle l',m'| \quad (18)$$

and

$$\begin{aligned} \rho' &= U_s \otimes U_i \rho U_i^\dagger \otimes U_s^\dagger \\ &= \sum_{l,m,l',m'} \rho_{l,m,l',m'} U_s \otimes U_i |l,m\rangle \langle l',m'| U_i^\dagger \otimes U_s^\dagger \\ &= \sum_{l,m,l',m'} \rho_{l,m,l',m'} |g_l, g_m\rangle \langle g_{l'}, g_{m'}|, \end{aligned} \quad (19)$$

by doing the reconstruction of ρ' we are also reconstructing ρ .

C. Non diagonal Elements

For simplifying the notation, we rewrite the $|h\rangle$ state, neglecting a global phase, as

$$|h\rangle = \cos\theta|g_+\rangle + e^{i\eta}\sin\theta|g_-\rangle, \quad (20)$$

where

$$\eta = \frac{2kd x}{(z - z_A)}, \quad (21)$$

and

$$\cos\theta \equiv |f_+(x, z)|, \sin\theta \equiv |f_-(x, z)|. \quad (22)$$

Note that, when we select a given value for the η angle at the detection plane located at a z distance, the value of the θ angle is completely defined. By considering the value of the experimental parameters: $z - z_A$, k , d , and a , it can be shown that the state $|h'\rangle = \cos\theta'|g_+\rangle + e^{i\eta'}\sin\theta'|g_-\rangle$, with $\eta' = \eta + \pi$, is orthogonal to the state $|h\rangle$ with a high accuracy, $|\langle h'|h\rangle| \leq 10^{-3}$, when $-\pi \leq \eta \leq \pi$. For practical purposes the base $\{|h\rangle, |h'\rangle\}$ are orthonormal because this value is less than the experimental error for determining the probabilities when different basis are considered.

The second type of coincidence measurements were done by positioning the signal detector, at the image plane, behind aperture “+” (“-”) of its double-slit and displacing transversely, the idler detector in the z -plane (See Fig. 1(c)). When the idler detector is at the transverse position $x = -0.688\text{mm}$ or $x = 0.688\text{mm}$, the detector selects the idler photons in the state given by Eq. (20) in which $\eta = \frac{-\pi}{2}$ ($|h_1\rangle$, $x_{-\pi/2} = -0.688\text{ mm}$) or $\eta' = \frac{\pi}{2}$ ($|h'_1\rangle$, $x_{\pi/2} = 0.688\text{ mm}$). Eq. (21) was used for calculating the x positions from η and η' . The fourth order interference pattern [25, 26], when the signal detector is fixed at “+” aperture and the idler is displaced transversely in the x -direction, is shown in Fig. 3. When the idler detector is at the transverse position $x = 0\text{ mm}$ or $x = 1.376\text{ mm}$, the detector selects the idler photons in the state given by Eq. (20) in which $\eta = 0$ ($|h_2\rangle$, $x_0 = 0\text{ mm}$) or $\eta' = \pi$ ($|h'_2\rangle$, $x_\pi = 1.376\text{ mm}$). With eight measured coincidence numbers, obtained from two interference patterns (signal detector behind aperture “+” or “-”), we determined the diagonal elements of the density operators written in the basis $\{|+, h_j\rangle, |+, h'_j\rangle, |-, h_j\rangle, |-, h'_j\rangle\}$, with $j = 1$ and 2 , which denotes the reconstructing base with $\eta = \frac{-\pi}{2}$ and $\eta = 0$, respectively. By repeating this detection procedure and reversing the roles of the signal and

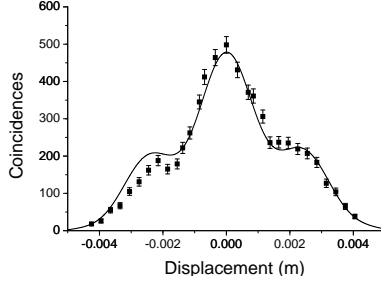


FIG. 3: Fourth order interference pattern as a function of D_i position. It was recorded when the detector signal was fixed behind the aperture “+”. The solid curve was obtained theoretically.

idler detectors (See Fig. 1(d)), we found the diagonal elements of another global density operators written in the basis $\{|h_j, +\rangle, |h_j, -\rangle, |h'_j, +\rangle, |h'_j, -\rangle\}$.

Relating the diagonal elements of the new density operators with the non diagonal elements of ρ , we determined: ρ_{++-+} (ρ_{-+++}), ρ_{+---} (ρ_{--+-}), ρ_{+++-} (ρ_{+-++}) and ρ_{-+--} (ρ_{---+}). We show below the explicit expressions that determine ρ_{++-+}

$$\Re(\rho_{++-+}) = \frac{(\tilde{\rho}_{\theta_1+\theta_1+} - \rho_{+++-} \cos^2 \theta_1 - \rho_{-+--} \sin^2 \theta_1) \cos \eta}{\sin 2\theta_1} - \frac{(\tilde{\rho}_{\theta_2+\theta_2+} - \rho_{+++-} \cos^2 \theta_2 - \rho_{-+--} \sin^2 \theta_2) \sin \eta}{\sin 2\theta_2}, \quad (23)$$

$$\Im(\rho_{++-+}) = -\frac{(\tilde{\rho}_{\theta_1+\theta_1+} - \rho_{+++-} \cos^2 \theta_1 - \rho_{-+--} \sin^2 \theta_1) \sin \eta}{\sin 2\theta_1} - \frac{(\tilde{\rho}_{\theta_2+\theta_2+} - \rho_{+++-} \cos^2 \theta_2 - \rho_{-+--} \sin^2 \theta_2) \cos \eta}{\sin 2\theta_2}, \quad (24)$$

where θ_j ($j = 1, 2$) are obtained from Eqs. (21) and (22), by setting $\eta = \frac{\pi}{2}$ ($j = 1$) and $\eta = 0$ for ($j = 2$) in Eq. (21) and substituting the values obtained for x in Eqs. (22).

In the third measurement type shown in Fig. 1(f), signal and idler detectors are positioned in the z-plane and the fourth-order interference patterns are measured. One of the detector is kept fixed while the other is scanned transversely for detecting the photon pairs in coincidence (see Fig. 4). Five interference patterns were measured with one of the detectors fixed at the transverse positions related to $\eta = -\pi, -\pi/2, 0, \pi/2$, and π by Eq. (21). This allows, by means of similar expressions to Eqs. (23) and Eq. (24), to completely determine the density operator ρ . These measurements correspond to local operations at both down-converted

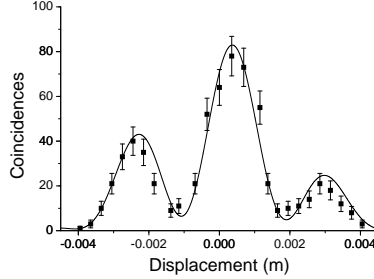


FIG. 4: Fourth order interference pattern as a function of D_s position. It was recorded when the detector idler was fixed at the transverse position which corresponds to $\eta' = \frac{\pi}{2}$ ($x = 0.688$ mm). The solid curve was obtained theoretically.

photons. The solid curves shown in Figs. 3, 4, and 5 were obtained theoretically. The photodetection coincidence rate $C(x_1, x_2)$ is proportional to $\text{Tr}(\rho_{\text{the}} E_1^\dagger E_2^\dagger E_2 E_1)$ [27], where ρ_{the} is shown in Eq. (7) with A and B being fit parameters. The electric field operators are built for each measurement type and can be seen in references [16, 20, 21].

Notice that for calculating the real and imaginary parts of ρ_{++-+} (Eqs. (23) and Eq. (24)) we use only two diagonal elements of the density operator written in the rotated basis: $\tilde{\rho}_{\theta_1+\theta_1+}$ and $\tilde{\rho}_{\theta_2+\theta_2+}$. We emphasize here that the scanning of one of the detectors can be seen as redundant information for the reconstruction. Only two measured points from each interference pattern were used for it. In total, we used 12 measured coincidence numbers, obtained from the second and third measurement type, and the four measured diagonal elements for obtaining all the non-diagonal elements of the density operator.

D. The Reconstructed Density Operator

By performing the quantum tomographic reconstruction, as described above, we found the following form for the density operator of our experiment

$$\rho = \begin{bmatrix} 0.028 & 0.083 + 0.004i & 0.081 + 0.005i & -0.129 + 0.062i \\ 0.083 - 0.004i & 0.468 & 0.444 - 0.058i & 0.097 - 0.008i \\ 0.081 - 0.005i & 0.444 + 0.058i & 0.462 & 0.096 - 0.006i \\ -0.129 - 0.062i & 0.097 + 0.008i & 0.096 + 0.006i & 0.042 \end{bmatrix}. \quad (25)$$

The elements of a density operator must satisfy the Schwarz inequality, i.e., $|\rho_{jk}| \leq \sqrt{\rho_{jj}\rho_{kk}}$, where $j, k = ++, +-, -+$ and $--$, if it really represents a quantum state. This is not our case for the matrix element ρ_{++--} , since it can be seen that $|\rho_{++--}| > \sqrt{\rho_{++++}\rho_{----}}$. The reason for that are the experimental fluctuations present in the coincidence measurements which can affect the final result as we discussed in the Introduction. This discrepancy can be reduced by increasing the detection time. Even though our reconstructed density matrix presents properties which are not fully compatible with the quantum state description, it is possible to show that in general it is consistent with the theory developed in Sec. II. This is done in the next section, where we also show experimental evidences of the good quality of our reconstruction.

IV. DISCUSSION AND CONCLUSION

The measured density operator shown in Eq. (25) can be approximately written as

$$\rho = 0.87|\Phi\rangle_{11}\langle\Phi| + 0.13|\Phi\rangle_{22}\langle\Phi|, \quad (26)$$

where the states $|\Phi\rangle$ are given by

$$\begin{aligned} |\Phi\rangle_1 = & 0.077e^{i\phi_1}|++\rangle + 0.704e^{i\phi_2}|+-\rangle \\ & + 0.699e^{i\phi_2}|-+\rangle + 0.099e^{i\phi_3}|--\rangle, \end{aligned} \quad (27)$$

and

$$\begin{aligned} |\Phi\rangle_2 = & 0.514|++\rangle + 0.502e^{i\theta}|+-\rangle \\ & + 0.501e^{i\theta}|-+\rangle + 0.483|--\rangle, \end{aligned} \quad (28)$$

with $\phi_1 \simeq \phi_2 \simeq \phi_3 \approx 4.2$ and $\theta = 0.07$.

However, the possibility to decompose the density operator, ρ , in terms of the projectors of a state, $|\Phi\rangle_1$, which has a high degree of entanglement and a state, $|\Phi\rangle_2$, that is of the form predicted by Eq. (6), is not sufficient for associating them with the states generated by each arm of the interferometer in our experiment. We still have to give an experimental evidence which corroborates with the expression of Eq. (26) as a reasonable approximation

for the quantum state of the twin photons, i.e., we need to show that the values of $A = 0.87$ and $B = 0.13$, obtained mathematically, are reasonable for the probabilities of generating these states in each arm.

We measured the values of A and B by blocking one of the arms of the interferometer and detecting the transmitted coincident photons through the signal and idler double-slits. A (B) is the ratio between the coincidence rate when arm 2 (arm 1) is blocked and the total coincidence rate when both arms are unblocked. From this measurement we obtained, $A = 0.85 \pm 0.03$ and $B = 0.15 \pm 0.03$, indicating a good agreement with the expression of Eq. (26) for the reconstructed density operator.

Another experimental evidence for the high value of A can be found in the fourth order interference patterns recorded with the third measurement procedure (See Fig. 1(e)). Since the state $|\Phi\rangle_1$ is almost a maximally entangled state we would expect to observe conditional interference patterns [25, 26] when both interferometer arms are unblocked. This would not be the case for high values of B . The conditionality observed in the interference patterns is showed in Fig. 5. The reason for having the probability of generating the state from the pump beam that cross arm 1 much higher than the probability of generating it from arm 2 is quite simple. The laser beam that cross arm 1 of the interferometer is focused at the slit's plane, and therefore, the spatial correlation of the generated photon pairs after the slits is larger than when the photon pairs are generated by the pump beam that cross arm 2 [15]. These values can be properly manipulated by inserting attenuators at the interferometer.

These experimental observations confirm the good quality of the QTR performed on the two photon state and allow us to consider the states $|\Phi\rangle_1$ and $|\Phi\rangle_2$ as good approximations for the states generated through the arm 1 and arm 2 of the interferometer used. Fig. 6 shows a histogram of the real part of the matrix elements of (a) the measured density operator (Eq. (25)), (b) the density operator given by Eq. (26) and (c) the predicted density operator shown in Sec. II. The agreement between the predicted and the measured density operator is good within the experimental errors. The largest error for the diagonal elements is only 3.5%. But, for the non-diagonal elements the propagated errors reaches 30% for their real parts and up to 65% for the imaginary parts, errors that can be decreased by increasing the detection time.

In conclusion, we have demonstrated that it is possible to generate a broad family of mixed states of spatial qudits by exploring the transverse correlation of the down-converted

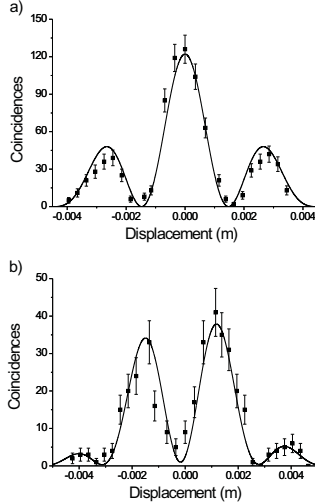


FIG. 5: Fourth order interference pattern as a function of D_s position. In (a), the detector idler was fixed at the transverse position $x = 0$ mm. In (b), it was fixed at the transverse position $x = 1376$ mm. The solid curves were obtained theoretically.

photons. A statistical mixture of spatial qubits were used to show the quantum tomographic reconstruction performed to characterize this type of composite system and measure its density operator. The process was discussed in details and experimental evidences for the good quality of the reconstruction performed were showed. Even though we had considered the state determination only for the case of qubits, we believe that it can be generalized and performed in a similar way for higher dimension systems in a mixed state. The importance of this work comes from the demand that the use of these systems for quantum communications requires the ability to characterize them.

V. ACKNOWLEDGMENTS

The authors would like to express their gratitude to Marcelo T. Cunha for having called their attention to this problem and initiating the discussions which culminated in this work. G. Lima, L. Neves and S. Pádua were supported by CAPES, CNPq, FAPEMIG and Milênio Informação Quântica. C. Saavedra and A. Delgado were supported by Grants Nos. FONDECYT 1061461 and Milenio ICM P02-49F. F. Torres was supported by MECESUP UCO0209. This work is part of the international cooperation agreement CNPq-CONICYT 491097/2005-

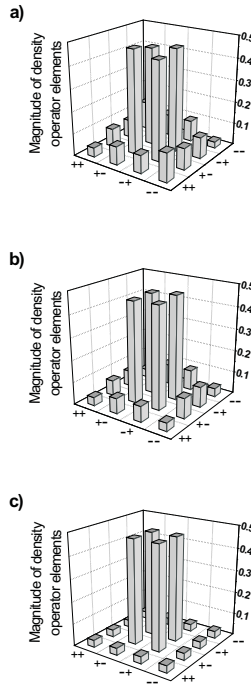


FIG. 6: Histogram of the real part of the matrix elements for (a) the measured density operator, (b) the density operator given by Eq. (26) and (c) the predicted density operator of Sec. II.

0.

-
- [1] C. H. Bennett *et al.*, Phys. Rev. Lett. **70**, 1895 (1993).
- [2] C. H. Bennett *et al.*, Phys. Rev. Lett. **69**, 2881 (1992).
- [3] W. K. Wootters, Phys. Rev. Lett. **80**, 2245 (1998).
- [4] S. Wallentowitz and W. Vogel, Phys. Rev. Lett. **75**, 2932 (1996).
- [5] P. J. Bardsroff, E. Mayr, and W. P. Schleich, Phys. Rev. A **51**, 4963 (1995); P. J. Bardsroff, C. Leichtle, G. Schrade, and W. P. Schleich, Phys. Rev. Lett. **77**, 2198 (1996); P. J. Bardsroff, E. Mayr, W. P. Schleich, P. Domokos, M. Brune, J. M. Raimond, and S. Haroche, Phys. Rev. A **53**, 2736 (1996).
- [6] T. J. Dunn, I. A. Walmsley, and S. Mukamel, Phys. Rev. Lett. **74**, 884 (1995).
- [7] K. Vogel and H. Risken, Phys. Rev. A **40**, 2847 (1989).

- [8] D. T. Smithey *et al.*, Phys. Rev. Lett. **70**, 1244 (1993).
- [9] H. Kuhn, D. G. Welsch, and W. Vogel, Phys. Rev. A **51**, 4240 (1995).
- [10] A. G. White, D. F. V. James, P. H. Eberhard, and P. G. Kwiat, Phys. Rev. Lett. **83**, 3103 (1999).
- [11] Z. Hradil, Phys. Rev. A **55**, R1561 (1997).
- [12] D. F. V. James, P. G. Kwiat, W. J. Munro, and A. G. White, Phys. Rev. A **64**, 052312 (2001).
- [13] L. Mandel and E. Wolf, *Optical Coherence and Quantum Optics*, Cambridge University Press, Cambridge (1995).
- [14] C. K. Hong, Z. Y. Ou, and L. Mandel, Phys. Rev. Lett. **37**, 2044 (1987).
- [15] L. Neves, S. Pádua, and Carlos Saavedra, Phys. Rev. A **69**, 042305 (2004).
- [16] L. Neves, G. Lima, J. G. Aguirre Gómez, C. H. Monken, C. Saavedra, and S. Pádua, Phys. Rev. Lett. **94**, 100501 (2005).
- [17] See also these qudit experimental works: E. V. Moreva *et al.*, Phys. Rev. Lett. **97**, 023602 (2006); S. P. Walborn *et al.*, Phys. Rev. Lett. **96**, 030501 (2006); S. S. R. Oemrawsingh, Phys. Rev. Lett. **95**, 240501 (2005); Malcolm N. O'Sullivan-Hale *et al.*, Phys. Rev. Lett. **94**, 220501 (2005); R. T. Thew, *et al.*, Phys. Rev. Lett. **93**, 010503 (2004); A. Vaziri, G. Weihs, and A. Zeilinger, Phys. Rev. Lett. **89**, 240401 (2002); J. C. Howell, A. Lamas-Linares, and D. Bouwmeester, Phys. Rev. Lett. **85**, 030401 (2002).
- [18] K. Blum, *Density Matrix Theory and Applications*, Plenum Press, New York (1981).
- [19] U. Leonhardt, *Measuring the Quantum State of Light*, Cambridge University Press, Cambridge (1997).
- [20] G. Lima, L. Neves, Ivan F. Santos, J. G. Aguirre Gómez, C. Saavedra, and S. Pádua, Phys. Rev. A **73**, 032340 (2006).
- [21] L. Neves, G. Lima, J.G. Aguirre-Gmez, C. Saavedra, and S. Pádua, Mod. Phys. Lett. **20**, 1 (2006); I. F. Santos, L. Neves, G. Lima, C. H. Monken, and S. Pádua, *et al.*, Phys. Rev. A **72**, 033802 (2005).
- [22] J. S. Bell, Physics 1, 195 (1964).
- [23] P. G. Kwiat *et al.*, Phys. Rev. Lett. **75**, 4337 (1995).
- [24] C. H. Monken, P. H. Souto Ribeiro, and S. Pádua, Phys. Rev. A **57**, 3123 (1998).
- [25] D. M. Greenberger, M. A. Horne, and A. Zeilinger, Phys. Today **46** (8), 22 (1993).
- [26] E. J. S. Fonseca, J. C. Machado da Silva, C. H. Monken, and S. Pádua, Phys. Rev. A **61**,

023801 (2000).

- [27] M. O. Scully and M. S. Zubairy, *Quantum Optics*, Cambridge University Press, Cambridge (1997).